MDPI

Article

Evolution and Mechanism Analysis of Terrestrial Ecosystems in China with Respect to Gross Primary Productivity

Hanshi Sun [1,2,3], Yongming Cheng [1,2,3], Qiang An [1,2,3] and Liu Liu [1,2,3,*]

1 State Key Laboratory of Efficient Utilization of Agricultural Water Resources, China Agricultural University, Beijing 100083, China; 2019309080206@cau.edu.cn (H.S.); s20213091740@cau.edu.cn (Y.C.); b20223090702@cau.edu.cn (Q.A.)
2 Center for Agricultural Water Research in China, China Agricultural University, Beijing 100083, China
3 College of Water Resources and Civil Engineering, China Agricultural University, Beijing 100083, China
* Correspondence: liuliu@cau.edu.cn

Abstract: The gross primary productivity (GPP) of vegetation stores atmospheric carbon dioxide as organic compounds through photosynthesis. Its spatial heterogeneity is primarily influenced by the carbon uptake period (CUP) and maximum photosynthetic productivity (GPP_{max}). Grassland, cropland, and forest are crucial components of China's terrestrial ecosystems and are strongly influenced by the seasonal climate. However, it remains unclear whether the evolutionary characteristics of GPP are attributable to physiology or phenology. In this study, terrestrial ecosystem models and remote sensing observations of multi-source GPP data were utilized to quantitatively analyze the spatio-temporal dynamics from 1982 to 2018. We found that GPP exhibited a significant upward trend in most areas of China's terrestrial ecosystems over the past four decades. Over 60% of Chinese grassland and over 50% of its cropland and forest exhibited a positive growth trend. The average annual GPP growth rates were 0.23 to 3.16 g C m^{-2} $year^{-1}$ for grassland, 0.40 to 7.32 g C m^{-2} $year^{-1}$ for cropland, and 0.67 to 7.81 g C m^{-2} $year^{-1}$ for forest. GPP_{max} also indicated that the overall growth rate was above 1 g C m^{-2} $year^{-1}$ in most regions of China. The spatial trend pattern of GPP_{max} closely mirrored that of GPP, although local vegetation dynamics remain uncertain. The partial correlation analysis results indicated that GPP_{max} controlled the interannual GPP changes in most of the terrestrial ecosystems in China. This is particularly evident in grassland, where more than 99% of the interannual variation in GPP is controlled by GPP_{max}. In the context of rapid global change, our study provides an accurate assessment of the long-term dynamics of GPP and the factors that regulate interannual variability across China's terrestrial ecosystems. This is helpful for estimating and predicting the carbon budget of China's terrestrial ecosystems.

Keywords: gross primary productivity; spatiotemporal evolutionary; interannual variability; carbon uptake period; photosynthetic capacity; China's terrestrial ecosystems

1. Introduction

Under the context of global climate change, there is growing attention on monitoring the spatial and temporal dynamics of terrestrial ecosystem gross primary productivity (GPP) and analyzing its attribution. Interannual variability serves as a crucial indicator of vegetation stability in response to external perturbations, significantly contributing to the assessment of the impacts of climate change on vegetation [1]. China is one of the world's fastest-greening countries, which alone accounts for 25% of the global net increase in leaf area between 2000 and 2017 with only 6.6% of the global vegetated area [2]. However, the driving mechanism behind the interannual variability of total vegetation primary productivity (GPP_{annual}) in China remains unclear, which is crucial for predicting the carbon cycle response to future climate change. Prior research has indicated that spatial heterogeneity of GPP was predominantly influenced by the duration of the carbon uptake

period (CUP) and the maximum photosynthetic productivity (GPP$_{max}$) [3]. Specifically, an earlier start of the growing season (SOS) and a later end of the growing season (EOS) can extend the duration of the growing season or alter the timing of photosynthesis activity [4,5], elucidating the spatial heterogeneity of GPP$_{annual}$ from a mechanistic perspective. Currently, plant phenology research, particularly focusing on SOS and EOS, has garnered widespread attention [3]. However, there are a limited number of studies focusing on GPP$_{max}$, a crucial factor in delineating ecosystem GPP capacity and influencing the seasonal patterns of atmospheric CO_2 concentrations, especially for terrestrial ecosystems of China with significant seasonality.

Grassland, cropland, and forest are crucial components of terrestrial ecosystems, playing a vital role in regulating greenhouse gas cycling and maintaining ecosystems' carbon balance [6]. According to the bulletin of the third major national land survey released by the State Forestry and Grassland Administration [7], grassland, cropland, and forest in China collectively occupy 85% of the total land area, constituting the main components of the terrestrial ecosystems. Given that most parts of China lie within the monsoon zone, with significant seasonal climate variations, China's terrestrial ecosystems exhibits high sensitivity to both climate change and human-induced disturbances [8]. Hence, the precise evaluation of spatial and temporal variations, coupled with an analysis of interannual GPP variability mechanisms in China's terrestrial ecosystems under the backdrop of climate change, can facilitate the estimation and prediction of carbon balance of these terrestrial ecosystems. In this study, we utilized multi-source GPP data as a proxy for vegetation growth to analyze the spatial and temporal characteristics of vegetation greening in China's terrestrial ecosystems over the past four decades. The GPP$_{max}$ was determined through the maximum value synthesis method, which illustrated the relationship between plant photosynthetic capacity and spatial-temporal variations in GPP. Furthermore, we further explored the mechanisms by which plant physiology and phenology influence GPP changes across different vegetation types.

2. Materials and Methods

2.1. Mask Extraction of Grassland, Cropland, and Forest in China

Moderate Resolution Imaging Spectroradiometer (MODIS) Global Vegetation Classification product (MODIS Collection5 MOD12Q1, Land Cover Data) provides globally categorized data classified by the International Geosphere-Biosphere Program (IGBP) Land Classification Rules. This dataset (500 m, annual) comprises 17 land cover categories, including 11 natural vegetation types, 3 categories for developed and urbanized areas, and 3 categories for non-vegetated land. Predominantly, these categories encompass grassland, cropland, and forest. For this study, we chose three land-use categories from the dataset: grassland, cropland, and forest. These categories were defined based on the IGBP land classification standard, with grassland represented by code 10, cropland by 12, and forest by codes 1, 2, 3, 4, 5, and 8.

Before evaluating the productivity of grassland, cropland, and forest in China, we generated 0.5° and 0.05° masks for Chinese grassland, cropland, and forest. Initially, utilizing the IGBP land classification system of the MOD12Q1 dataset spanning from 2001 to 2018, we systematically extracted image elements corresponding to land-use types across China at a 500 m resolution annually. The components were then integrated into 0.05° resolution images utilizing ArcGIS 10.8. Subsequently, the extracted elements from these images were spatially superimposed across multiple time periods. Elements present in at least two-thirds of the 18-year period (i.e., 12 years) were designated as 0.05° masks representing grassland, cropland, and forest [9].

To align with the 0.5° resolution data of the model GPP dataset, we constructed a 0.5° resolution grid of land use types for the Chinese region. The approach involved tallying the proportion of grassland, cropland, and forest image elements (0.05°) within each 0.5° grid cell. Subsequently, image elements corresponding to land use types exceeding 60%

within each grid cell were filtered and designated as 0.5° grassland, cropland, and forest masks. The processing details for this step are shown in Figure 1.
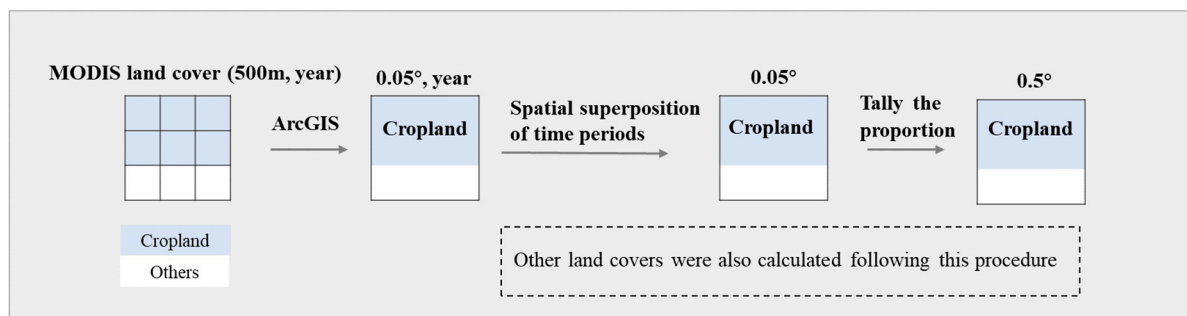

Figure 1. Steps for processing raw land-use data into 0.05° and 0.5° grids.

The following mask images of China's terrestrial ecosystems was created based on the above two methods (Figure 2).
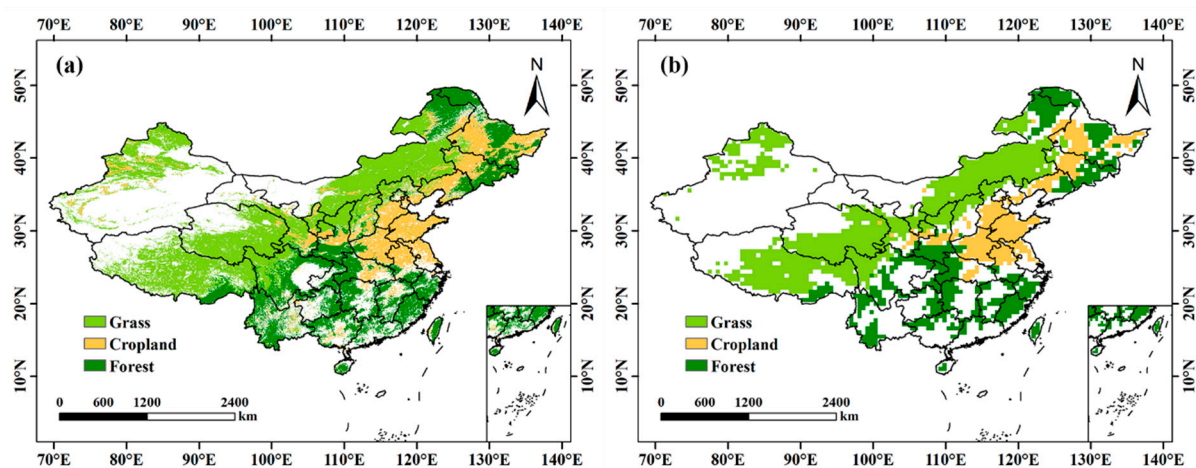

Figure 2. Masking results at different resolutions for China's terrestrial ecosystems. (**a**) is the map with a resolution of 0.05°; (**b**) is the map with a resolution of 0.5°.

The above approach was taken mainly because the grassland, cropland, and forest images have been converted to other land use types in the past 18 years in China. To facilitate a more accurate study of the spatial and temporal dynamics of China's terrestrial ecosystems, it is imperative to disregard image elements exhibiting conspicuous alterations in land use types. The 0.05° and 0.5° masks generated in this study were employed to extract additional GPP and hydrometeorological data pertaining to China's terrestrial ecosystems [10,11].

2.2. GPP Data

The Multi-scale Synthesis and Terrestrial Model Intercomparison Project (MsTMIP) is a model comparison program aimed at developing globally gridded estimates of carbon, energy, and hydrological fluxes among different models of land and atmosphere [12]. To ensure consistent and comparable model results, the MsTMIP has assembled benchmark reference driver data sets, including standard weather drivers, remotely sensed phenology, biome classification, and land-use history to provide GPP output products in historical periods [13]. In the newly released model simulation results (https://daac.ornl.gov/NACP/guides/NACP_MsTMIP_TBMO_V2.html, accessed on 23 January 2024), MsTMIP provides monthly data values at a spatial resolution of 0.5° and a temporal resolution spanning from 1901 to 2010. Based on previous theoretical studies [14], four terrestrial

ecosystem models were selected for inclusion in the MsTMIP multi-scenario model for this study: Community Land Model version 4 (CLM4) [15], CLM4-Variable Infiltration Capacity model (CLM4-VIC) [16], Dynamic Land Ecosystem Model (DLEM) [17], and Integrated Science Assessment Model (ISAM) [18]. Despite the standardized protocol used to derive initial conditions, different models show a high degree of variation for GPP, so we applied an ensemble average of the four GPP model data to reduce the uncertainty of the GPP data.

The Inter-Sectoral Impact Model Intercomparison Project (ISIMIP) also is a model comparison plan. The objective is to establish a framework for comparing risk models globally and regionally across various sectors, facilitating coordinated multi-sectoral assessments of diverse risks and their cumulative impacts to support decision-making on adaptation and mitigation at both the global and regional levels [19]. This study selected four sets of monthly GPP data, each with a spatial resolution of 0.5° and a temporal resolution spanning from 1901 to 2005, adhering strictly to the ISIMIP2b standard protocol. The meteorological forcing data utilized are from IPSL-CM5A-IR: CARbon Assimilation In the Biosphere (CARAIB) [20], Lund-Potsdam-Jena: General Ecosystem Simulator (LPJ-GUESS) [21], Lund-Potsdam-Jena managed Land (LPJmL) [22], and Organizing Carbon and Hydrology in Dynamic EcosystEms: Dynamic Global Vegetation Model (ORCHIDEE-DGVM) [23]. Similar to the handling of MsTMIP data, we applied an ensemble average of the four GPP model data to reduce uncertainty of the GPP data.

Global Land Surface Satellite (GLASS) products, derived from multi-source remote sensing data and ground-truthing data, offer long-term, high-precision global surface remote sensing data. They serve as a dependable foundation for investigating global environmental change, facilitating the global, intercontinental, and regional monitoring of atmospheric dynamics, vegetation cover, water bodies, and more. These products, when integrated with climate change parameters like temperature and precipitation, enable the analysis of global change [24]. GPP, one of GLASS's key products, spans a lengthy period (1982–2018) with high temporal and spatial resolution (0.05°, 8 days), making it optimal for analyzing temporal and spatial variations in GPP. The GLASS GPP algorithm is based on the Eddy Covariance-Light Use Efficiency (EC-LUE) model, which originally relies on four variables: remotely sensed NDVI, PAR, air temperature, and Bowen's ratio [25]. The updated GLASS GPP product incorporates additional environmental variables, including atmospheric CO_2 concentration, direct and scattered radiation fluxes, and atmospheric water vapor pressure deficit [26], to better capture long-term trends in GPP.

Additionally, to mitigate the uncertainty arising from individual remote sensing datasets, we employed the Multisource Data Synergized Quantitative (MuSyQ) algorithm for GPP assessment [27]. Unlike GLASS GPP, MuSyQ GPP incorporates a clear-sky index, substantially enhancing GPP accuracy for remote sensing observations [28]. MuSyQ GPP data (0.05°, 8 days) are accessible at https://zenodo.org/records/3996814#.Y5V46FFBxD-, accessed on 25 January 2024.

To verify the accuracy of the model and remote sensing data in estimating GPP, this study utilized observation data from flux towers in China, comparing them with the model and remote sensing data for validation. The flux tower data can be accessed at https://fluxnet.org/, accessed on 23 June 2024. The methodology involved obtaining GPP observation data from the flux towers and determining their corresponding longitude and latitude. These coordinates were then used to locate the matching grids in the model and remote sensing data, from which data for the same years were extracted for comparison and analysis. The results (Figure 3) indicated that the GPP values from the flux tower data closely match those from the model and remote sensing data, exhibiting similar variation trends. This concordance verified the accuracy and reliability of the model and remote sensing data used in this study.
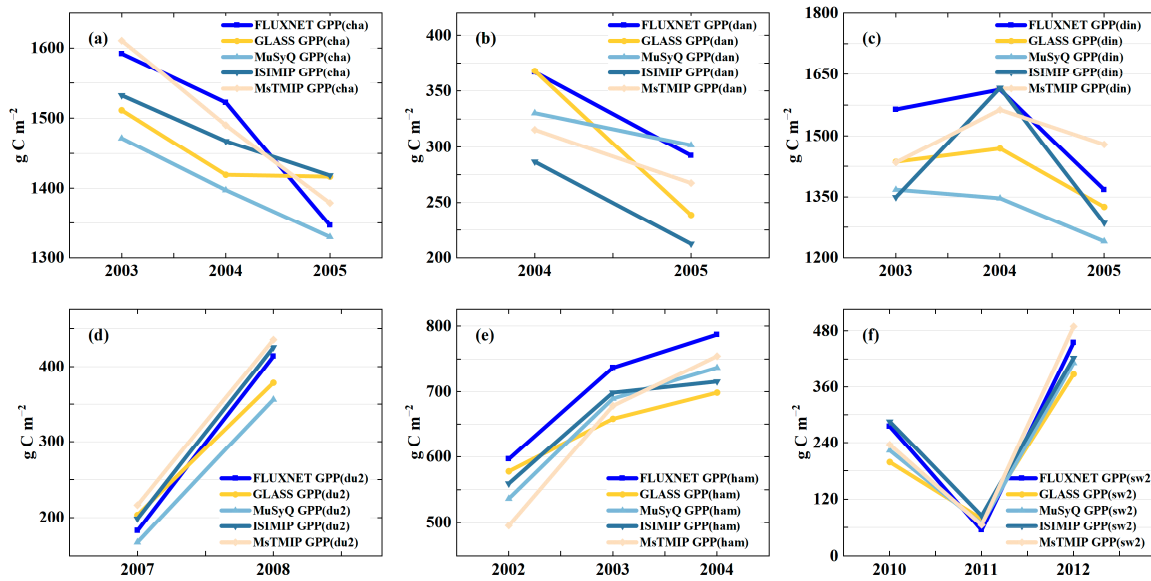
Figure 3. Comparison of flux tower data with model and remote sensing data. (**a**) represents the Changbai Mountain site (128.0958° E, 42.4025° N); (**b**) represents the Dangxiong site (91.0664° E, 30.4978° N); (**c**) represents the Dinghushan site (112.5361° E, 23.1733° N); (**d**) represents the Duolun_grassland (D01) site (116.2836° E, 42.0467° N); (**e**) resents the Haibei Alpine Tibet site (101.1800° E, 37.3700° N); and (**f**) represents the Siziwang Grazed (SZWG) site (111.8971° E, 41.7902° N).

2.3. Calculation of Peak Photosynthesis Productivity and Carbon Uptake Period

Peak photosynthetic productivity, represented by the highest annual gross primary productivity value, was obtained by synthesizing GPP data using the maximum value synthesis method. The equation used to derive GPP_{max} data for the entire year is as follows.

$$GPP_{max} = Max(GPP_i) \tag{1}$$

where GPP_{max} represents the maximum value of GPP in the year corresponding to a given grid, and GPP_i is the ith eight-day (or monthly value) GPP data.

Piao et al. [29] proposed fitting the intra-annual vegetation GPP dynamics using the monadic six-dimensional polynomial. They identified the start of the phenological period (SOS) as the position with the largest derivative between days 30–180 and the end of the phenological period (EOS) as the position with the smallest derivative between days 181 and 365 [30]. The phenological period length, also termed as the number of carbon dioxide uptake days (CUP), was calculated as the difference between the EOS and SOS.

2.4. Partial Correlation Analysis

Partial correlation analysis aims to explore relationships among multiple variables by isolating their direct associations from the influences of other variables, thereby enabling a more precise evaluation of potential causal relationships. The relationship between GPP, phenological period length, and peak photosynthesis productivity growth power was examined for each grid using partial correlation coefficient analysis. The partial correlation coefficient, denoted as 'r', ranged from −1 to 1, indicating the strength and direction of the correlation. A positive 'r' value (>0) indicates a positive correlation between the variables, while a negative 'r' value (<0) indicates a negative correlation.

$$r_{XY \cdot Z} = \frac{r_{XY} - r_{XY} r_{XZ}}{\sqrt{\left(1 - r_{YZ}^2\right)\left(1 - r_{XZ}^2\right)}} \tag{2}$$

where $r_{XY·Z}$ represents the degree of correlation between another variable and GPP after controlling for plant phenology or peak photosynthesis productivity growth force, and r_{XY}, r_{XZ}, and r_{YZ} represent the correlation coefficients between different variables, respectively.

We separately controlled for CUP and GPP_{max} and then compared the absolute values of the partial correlation coefficients between GPP and GPP_{max}, as well as between GPP and CUP. Then, we identified the elements dominating the interannual variation of GPP for each grid.

3. Results

3.1. Spatio-Temporal Variation Characteristics of GPP from Different Data Sources

In terms of spatial variation characteristics (Figure 4), GPP simulated by ISIMIP for grassland, cropland, and forest in China from 1982 to 2018 indicated that 71.99%, 51.97%, and 98.49% area of grassland, cropland, and forest lands exhibited a rising trend, with the proportions that showed a significant increasing trend being 58.89%, 20.79%, and 87.79%. Similarly, in MsTMIP, 61.74%, 57.58%, and 58.36% of the area of grassland, cropland, and forest lands showed increasing trends of GPP, with the proportions that showed a significant increasing trend being 20.80%, 13.48%, and 11.71%. However, there was a decreasing trend of grassland GPP in Xinjiang and cropland GPP in the North China plains, while MsTMIP GPP showed a decreasing trend in the cropland of Northeast China and forest near the Sichuan basin. The two remote sensing GPP datasets exhibited similar spatial variation trends in grassland, with over 81% of the area displaying an increasing trend from 1982 to 2018, and the proportions of GLASS and MuSyQ grass GPPs that showed a significant upward trend were 53.63% and 50.51%, respectively. However, the trends of cropland and forest GPPs in China differed. In the MuSyQ dataset, a higher percentage of grid points showed an increasing trend, reaching 89% for cropland GPP and 84% for forest GPP, respectively. This phenomenon is likely due to the inclusion of the Clearness Index (CI) in the MuSyQ dataset. The CI indirectly represents the varying proportions of direct and indirect radiation in incident solar radiation, incorporating the impacts of light, moisture, and temperature conditions on light energy utilization [28]. This leads to an enhanced light use efficiency (LUE) when compared to the GLASS dataset, consequently affecting the dataset's GPP.

The absolute variation in GPP values across different sources was relatively large (Figure 5), yet the overall trend was upward, reflecting the inter-annual fluctuations of different vegetation types in China's terrestrial ecosystems. Grassland GPP growth rates in China ranged from 0.23 to 3.16 g C m^{-2} year^{-1} and cropland GPP growth rates in China ranged from 0.40 to 7.32 g C m^{-2} year^{-1}; the forest GPP in China exhibited the most pronounced increasing trend, with an average growth rate ranging from 0.67 to 7.81 g C m^{-2} year^{-1} (Figure 5d). We observed a higher increasing rate in GPP in cropland compared to grassland. The increase in cropland GPP is closely linked to human activities. In recent years, modern farming practices like precision irrigation, optimal fertilization, and the cultivation of high-yield crop varieties have significantly enhanced photosynthetic efficiency and GPP [31]. Furthermore, climate change, including warmer temperature, longer carbon uptake period, and higher CO_2 concentration, has also occurred. Cropland is more sensitive to temperature and CO_2 levels [32], resulting in a higher GPP increase compared to grassland. In summary, both model-based and remote sensing-based spatial and temporal analyses confirmed a significant increase in GPP across China's terrestrial ecosystems over the last four decades, and these ecosystems have become more efficient carbon sinks compared to the previous century.
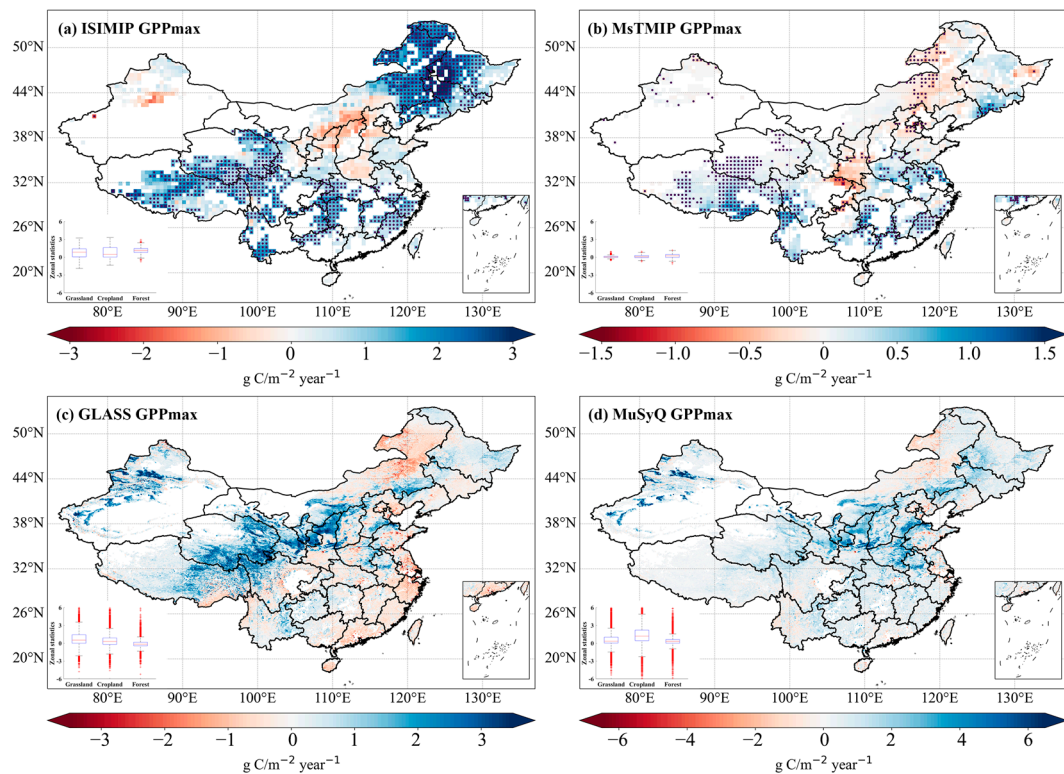
Figure 4. Spatial patterns of GPP changes of terrestrial ecosystems in China from 1982 to 2018 based on models and remote sensing observations. (**a**,**b**) are trends on grid-wise GPP changes averaged by the multi-model combinations of ISIMIP and MsTMIP, respectively. The dots in the graph represent that this point passes the significance test of $p < 0.05$. (**c**,**d**) are trends on grid-wise GPP changes averaged by GLASS and MuSyQ datasets, respectively. The regional average trend values are counted as box plots in the lower left corner. Data points that are more than 1.5 times the interquartile range of the first and third quartiles are marked as outliers, which are indicated by red dots in the figure.
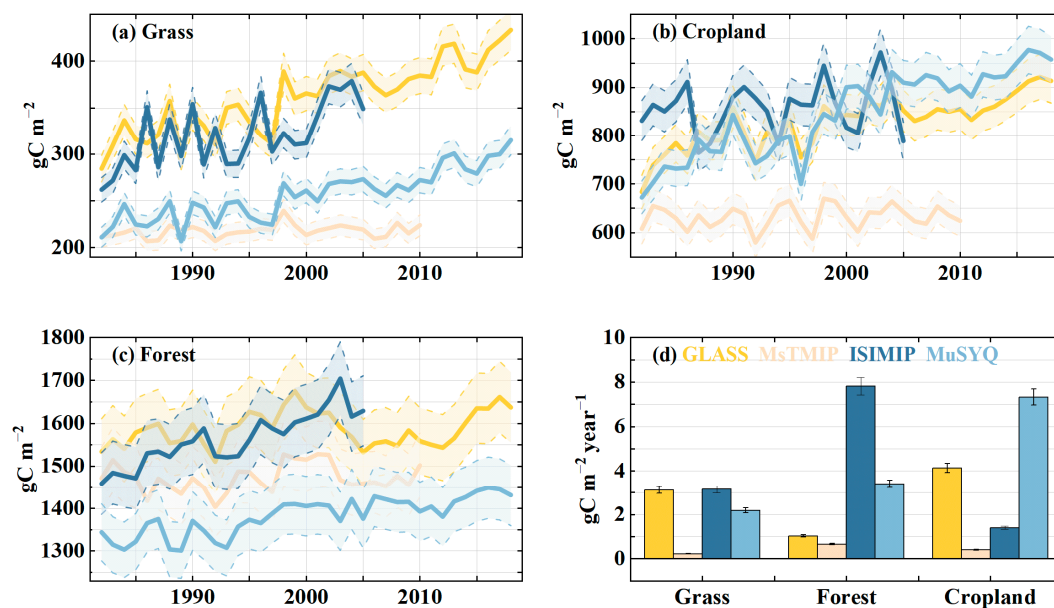

Figure 5. Interannual changes in model and remotely sensed GPP for China's terrestrial ecosystems from 1982 to 2018. (**a**–**c**) Annual GPP values of China's terrestrial ecosystems; (**d**) average slopes of the long-term trends of GPP in China's terrestrial ecosystems.

3.2. Spatial and Temporal Trends in GPP$_{max}$ from Different Data Sources

Plant photosynthesis is crucial for understanding plant physiology and its response to environmental changes. As the maximum photosynthetic carbon uptake represents the important characteristics of plant photosynthesis, it can be used as an indicator of plant physiology. The monthly-scale GPP data for China's terrestrial ecosystems was analyzed to extract the maximum value for each year, termed GPP$_{max}$, to map the spatial pattern of long-term trends. The spatial patterns of the GPP$_{max}$ trends derived from both model-based simulations and remote sensing closely mirrored those of the overall GPP data. All trends exhibited significant increases over time.

Discrepancies in GPP$_{max}$ were observed between model simulations and remote sensing data from different sources (Figure 6). In the ISIMIP dataset, GPP$_{max}$ exhibited rapid growth, averaging $1 \text{ g C m}^{-2} \text{ year}^{-1}$ across most regions except the Xinjiang and the Loess Plateau grassland, with a particularly notable increase in the northeastern cropland, whereas the MsTMIP GPP$_{max}$ simulated by the same model exceeded $1 \text{ g C m}^{-2} \text{ year}^{-1}$ solely in the grassland areas of the southern Tibetan Plateau and the cropland of North China plain, with a less pronounced upward trend in the Northeast cropland. The spatial trend patterns of GPP$_{max}$ in Chinese grassland derived from two remote sensing-based models were largely consistent. Both models indicated a decline in GPP$_{max}$ within the grassland of eastern Inner Mongolia. Moreover, the forest of southeastern China exhibited an increasing trend in GPP$_{max}$, which was not captured by the GLASS dataset. This showed the inadequacy of relying solely on one data source for a comprehensive analysis of GPP and GPP$_{max}$ trends. Multiple GPP datasets are essential for comparison to achieve a detailed understanding of the spatial and temporal dynamics of the ecosystem GPP in China.
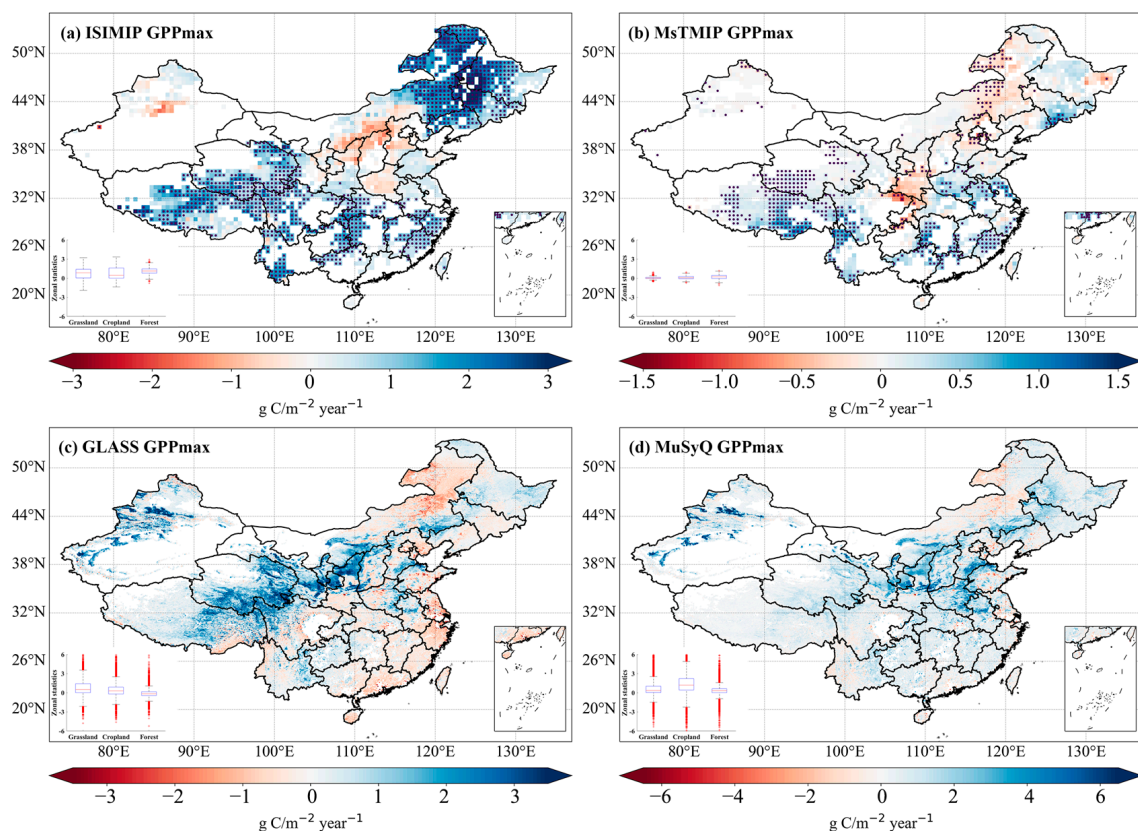

Figure 6. Spatial patterns of GPPmax changes in China's terrestrial ecosystems over the past four decades based on model and remote sensing observations. (**a**,**b**) are the direction and magnitude of

GPPmax changes averaged by the multi-model combinations of ISIMIP and MsTMIP, respectively. The dots in the graph represent that this point passes the significance test of $p < 0.05$. (**c**,**d**) are the direction and magnitude of GPPmax changes driven by GLASS and MuSyQ datasets, respectively. The regional average trend values are counted as box plots in the lower left corner. Data points that are more than 1.5 times the interquartile range of the first and third quartiles are marked as outliers, which are indicated by red dots in the figure.

When comparing the interannual changes in GPP_{max} of China's terrestrial ecosystems, differences emerged between the model and remote sensing GPP_{max}. Specifically, the GPP_{max} values from MsTMIP for cropland and forest were lower than those from the other three data sources, but overall, there was a more consistent fluctuating increase (Figure 7). Grassland GPP_{max} ranges from 60 to 120 g C m^{-2}, while cropland GPP_{max} typically ranges between 180 and 240 g C m^{-2}, with the exception of the MsTMIP dataset. Forest remote sensing GPP_{max} remained relatively constant at approximately 250 g C m^{-2}. Most grassland areas and cropland as well as forest, except for individual data from a few regions, exhibited GPP_{max} growth rates exceeding 0.15 g C m^{-2} $year^{-1}$, 0.09 g C m^{-2} $year^{-1}$, and 0.18 g C m^{-2} $year^{-1}$, respectively.
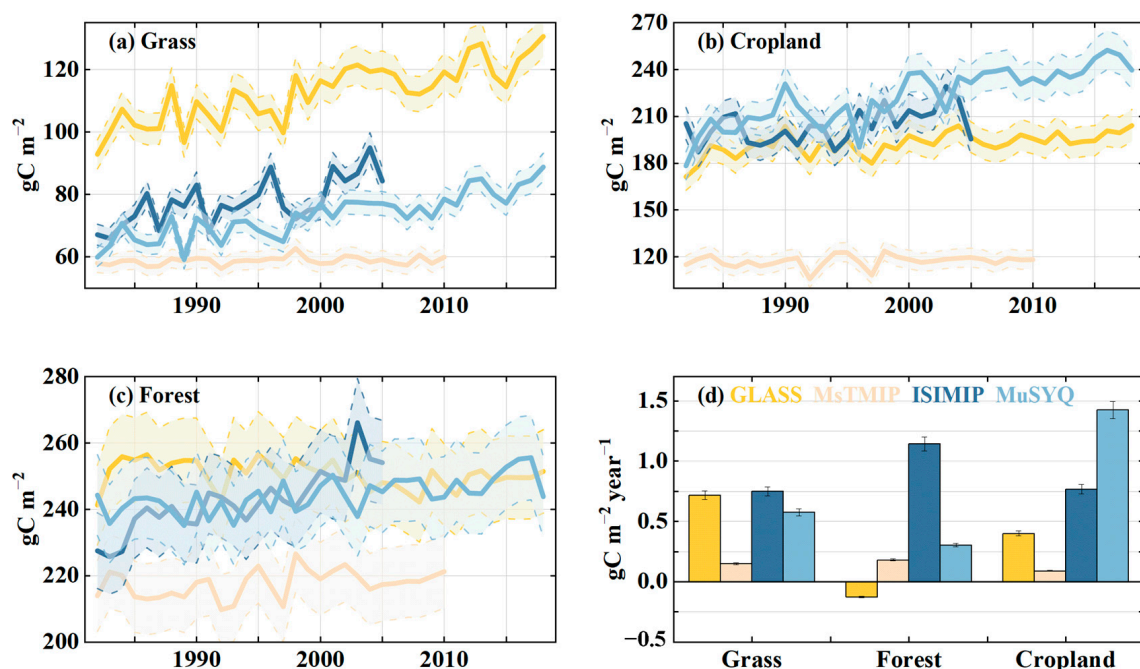

Figure 7. Interannual changes in the model and remotely sensed GPP_{max} for China's terrestrial ecosystems from 1982 to 2018. (**a**–**c**) Annual GPP_{max} values of China's terrestrial ecosystems; (**d**) average slopes of the long-term trends of GPP_{max} in China's terrestrial ecosystems.

3.3. Plant Physiology, Not Phenology, Dominates GPP Variability

GPP_{max} is considered the most reliable proxy for peak photosynthetic productivity and is closely related to plant physiology. CUP represents the duration of CO_2 absorption by vegetation throughout the year and is closely related to plant phenology. Although the effects of plant phenology and physiology on the interannual variability of GPP are evident, the magnitude of their influence remains uncertain [3]. Previous studies in North America, at both the ecosystem and regional scales, have indicated that the long-term trend and interannual variability of GPP is regulated by GPP_{max} [4], yet this assertion has not been validated in China.

In this study, prior to assessing the impact of plant phenology and physiology on interannual GPP, we conducted a comprehensive analysis of the temporal and spatial variations in GLASS GPP_{max} at both the 8-day and monthly scales. The standardized values of GPP_{max} over 8-day and monthly periods exhibited consistent trends, validating

the suitability of the GLASS GPP$_{max}$ dataset for subsequent analyses at an 8-day temporal resolution (Figure 8).
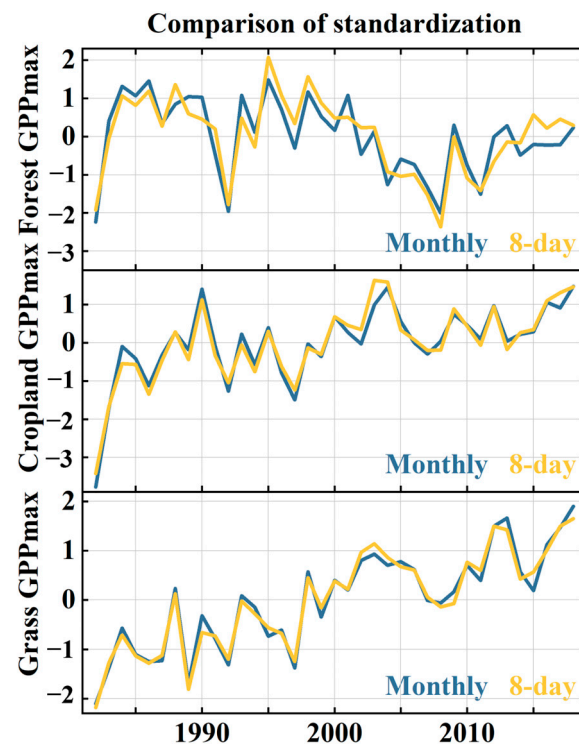

Figure 8. Comparison of long-term in GLASS grassland, cropland, and forest 8-day GPP$_{max}$ and monthly values.

Next, we examined the spatial variation characteristics of 8-day GPP$_{max}$ and observed a pronounced increase in China's terrestrial ecosystems' GPP$_{max}$. The average inter-annual variability of GPP$_{max}$ was 0.026 g C m^{-2} year^{-1}, 0.018 g C m^{-2} year^{-1}, and -0.04 g C m^{-2} year^{-1} for grassland, cropland, and forest, respectively. In particular, the increasing trend was evident in the grassland of the Loess Plateau, the grassland of Tibetan Plateau, and the cropland of North China Plain (Figure 9a), where the GPP$_{max}$ growth rate exceeded 0.1 g C m^{-2} year^{-1} in most of these regions. This could be attributed to significant vegetation restoration projects on the Loess Plateau, gradual climate warming and humidification on the Tibetan Plateau, and agricultural expansion on the North China Plain, all contributing to a faster increase in GPP$_{max}$ in these regions compared to others [33,34]. Upon comparing GPP$_{max}$ changes over the past four decades, the emergence date of GPP$_{max}$ in Chinese grassland, cropland, and forest has not significantly shifted, except for a slight delay in some Loess Plateau grassland and an earlier emergence in the grassland of Inner Mongolia and the forest of southern China (Figure 9b). In summary, 8-day GPP$_{max}$ served as a reliable indicator of peak ecosystem productivity, allowing for the construction of stable metrics using GLASS GPP$_{max}$ to assess the influence of plant physiology and phenology on interannual GPP in subsequent analyses.

Interannual changes of GPP in Chinese grassland were primarily controlled by GPP$_{max}$, with very limited influence (less than 1%) from CUP (Figure 10a). This indicated that the grassland ecosystems rely more on climatic factors such as precipitation and temperature, while their capacity to utilize soil moisture and nutrients remains relatively stable. For cropland, GPP changes were predominantly influenced by GPP$_{max}$, with 8% of interannual GPP changes attributed to CUP, mainly in the North China Plain (Figure 10b). In over 15% of forested areas in China, CUP played a significant role, especially in the Qinling, Hengduan, and Changbai mountain ranges, possibly due to the dominant role of physiological factors in vegetation growth in these regions as a result of soil moisture and temperature conditions

at high altitudes. The interannual variation of GPP in the remaining forested regions was still mainly controlled by GPP$_{max}$ (Figure 10c). There may be significant differences in the drivers of GPP change across geographic regions and vegetation types, and these differences were influenced not only by geographic conditions but also by vegetation type and region-specific ecosystem interactions. Overall, plant physiology, rather than phenology, predominated in driving the interannual variation of GPP in China's terrestrial ecosystems.
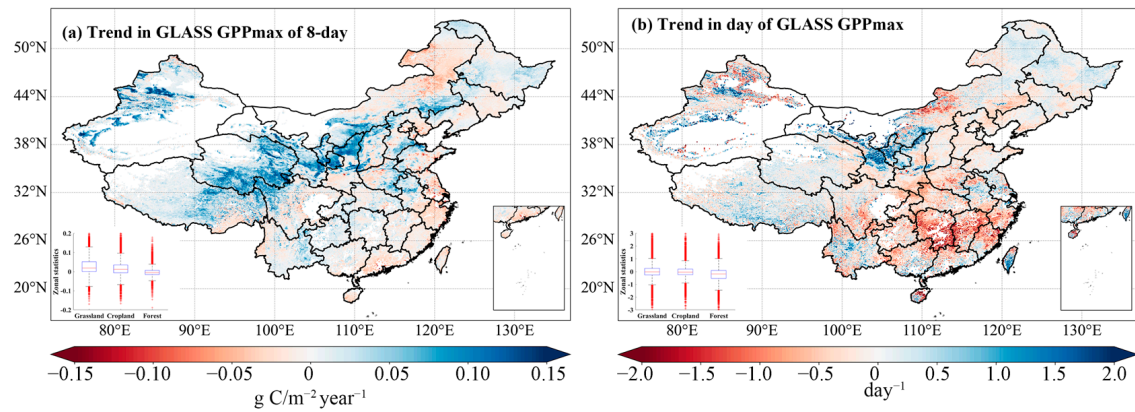

Figure 9. Spatial variation trend of (**a**) GPP$_{max}$ based on 8-day GLASS from 1982 to 2018; (**b**) spatial variation trend pattern of the dates on which GPP$_{max}$ is located. The regional average trend values are counted as box plots in the lower left corner. Data points that are more than 1.5 times the interquartile range of the first and third quartiles are marked as outliers, which are indicated by red dots in the figure.
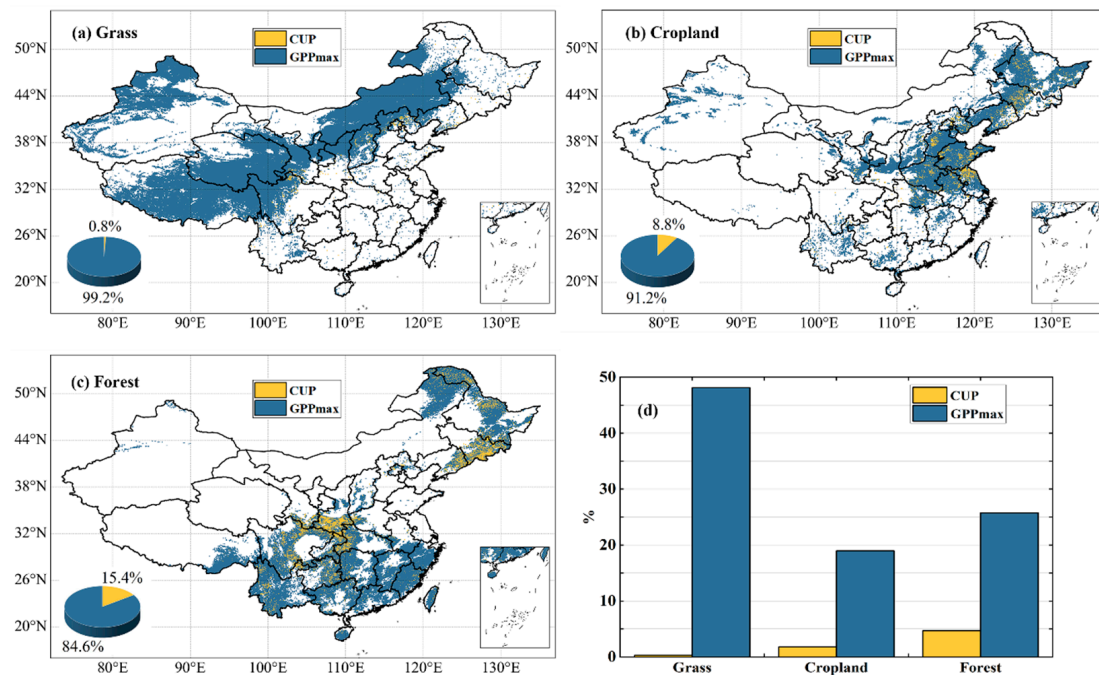

Figure 10. Results of the partial correlation analysis of the GLASS dataset (yellow indicates that the GPP trend change is controlled by CUP, blue indicates that the trend change is controlled by GPP$_{max}$). (**a**–**c**) are the results of partial correlation analyses for China's terrestrial ecosystems, respectively. (**d**) is the proportion of CUP and GPP$_{max}$ in the three ecosystems controlling changes in GPP.

4. Discussion

4.1. China's Terrestrial Ecosystems' GPP Growth Contributes to Global Warming Mitigation

Given China's position as the world's second-largest historical emitter of CO_2 [35], a precise evaluation of the CO_2 absorption capacity within China's terrestrial ecosystems holds profound implications for future endeavors towards carbon neutrality, carbon peaking, and environmental policy development. Our findings indicated a significant increase in the GPP of China's terrestrial ecosystems from 1982 to 2018, aligning with prior research [36–38]. However, adverse changes were solely detected in the eastern Inner Mongolian grassland and the North China Plain. Fang et al. reported that China's terrestrial ecosystems absorbed 20.8–26.8% of carbon emissions from Chinese industries [39], implying that various management practices including afforestation, grassland protection, agricultural system reform, and conservation tillage have been instrumental in carbon sequestration since the mid-1970s [40]. Enhancing vegetation restoration can increase the carbon sequestration capacity of terrestrial ecosystems, offering an effective approach to tackle global climate change and attain carbon neutrality goals. In summary, over the past four decades, China's terrestrial ecosystems' GPP has significantly increased, playing a crucial role in mitigating the rate of global warming.

4.2. Multi-Source Data and Methods Reveal a More Comprehensive Picture in China's Terrestrial Ecosystems

Modeling and remote sensing data are commonly used to investigate ecosystem GPP dynamics across various spatial and temporal scales. However, different GPPs are prioritized differently in estimation and monitoring [41]. Terrestrial ecosystem models driven by meteorological factors are frequently employed for estimating terrestrial ecosystem GPP. While these models can accurately simulate terrestrial ecosystem dynamics and their interactions with other Earth systems, they are susceptible to uncertainties stemming from the model's sensitivity to meteorological parameters and the uncertainty associated with meteorological datasets [42]. Furthermore, terrestrial ecosystem models are based on the current academic knowledge of the processes of the global carbon cycle and may have some limitations, which in turn lead to uncertainty in the model results [43]. Remote sensing GPP products, on the other hand, rely on a globally parameterized GPP model and are derived from long time series of remote sensing data, ultimately producing remotely sensed products. However, these remote sensing data are prone to atmospheric interference and may produce misleading signals under vegetation stress conditions, such as green canopies that are not actively photosynthesizing [44]. Furthermore, satellite remote sensing data can only offer momentary spectral information, and the GPP derived from sensor photography and data processing remains inadequate.

Previous studies have shown that choosing only model data or remote sensing data, but not both, to analyze vegetation dynamics can lead to controversial conclusions. There are significant uncertainties among different datasets, and even within the same model comparison program, GPP values can vary greatly between different models. In addition, analyzing only spatial trends in GPP across grids and ignoring trend changes in annual average GPP may lead to some uncertainty in the results of the study. Therefore, we suggest utilizing multivariate data, including both models and remote sensing, to analyze the spatial and temporal dynamics of past, present, and future GPP across China's terrestrial ecosystems, aiming to comprehensively assess the carbon balance dynamics. We also recommend that a combination of annual average GPP and spatially gridded GPP trend analyses should be used to jointly characterize the changing state of vegetation GPP in China's terrestrial ecosystems. By avoiding reliance on a single data source and method, which could potentially yield misleading conclusions, this paper aims to offer a more comprehensive and realistic portrayal of productivity changes in China's terrestrial ecosystems.

4.3. The Physiological Role of Plant Should Be Given More Attention to Better Explain Inter-Annual Variability in GPP

Previous research indicates that annual changes in GPP result from various biotic and abiotic factors, primarily alterations in plant phenology and physiological processes [45,46]. In this study, through partial correlation analyses of plant phenology and peak photosynthetic productivity with interannual GPP changes, we ascertained that plant physiology outweighs phenology in determining GPP's long-term trend. The importance of plant phenology on seasonal and annual GPP variability has been shown in many studies [45,47,48], Seasonal phenological events, such as leaf-out and senescence, directly influence the length of the growing season and hence the period during which photosynthesis can occur. However, phenological changes cannot explain GPP reduction caused by climate extreme events, which account for the majority of global inter-annual variability in GPP [49]. For instance, extreme droughts or heatwaves can lead to immediate reductions in photosynthetic activity due to stomatal closure and other stress responses, regardless of phenological stage.

Due to the direct correlation between photosynthetic physiology and carbon assimilation, GPP_{max} in this study is closely related to GPP and accounts for most of its interannual variability. The maximum rate of photosynthesis (GPP_{max}) is primarily determined by factors such as leaf area index (LAI), chlorophyll content, and enzyme activities involved in the Calvin cycle. Results from biased correlation analyses by Xia et al. [3] also indicated that GPP_{max} contributes more to GPP's interannual variability than CUP in most ecosystem types. This suggest that while the duration of the photosynthetically active period (CUP) is crucial, the efficiency and capacity of photosynthesis during this period are more significant determinants of overall productivity.

It has been suggested that vegetation GPP_{max} has the potential to continue to increase, and modern plant trait measurements have found that leaf photosynthetic capacity varies greatly among vegetation functional types. These variations can be attributed to differences in stomatal conductance, nitrogen use efficiency, and the capability of plants to acclimatize to changing environmental conditions through physiological adjustments. Studies under warming scenarios have also shown that the relationship between vegetation growth activity and temperature variability tends to weaken, and so does the extension of the CUP [50]. This may be due to the saturation of photosynthetic rates at higher temperatures and the increased occurrence of thermal stress, which can offset the benefits of longer growing seasons. The role of controlling vegetation carbon sequestration by GPP_{max} will be further strengthened. Given that GPP_{max} exhibits trends over time, greater focus should be placed on plant physiological changes to better explain GPP variability and enhance monitoring in terrestrial ecosystems.

4.4. Limitations and Uncertainties

Firstly, this study focuses primarily on how plant physiology and phenology affect GPP. However, ecohydrological factors, such as precipitation, temperature, and soil moisture, are also crucial for GPP growth. The situation and determinants vary across different vegetation types. For instance, Zhao et al. found that temperature is the primary factor influencing grassland growth in China. As latitude decreases, the correlation between GPP and temperature weakens, and moisture becomes the most significant limiting factor [51]. For cropland, Zhao et al. observed a significant positive correlation between GPP and precipitation in over half of the agricultural areas. Soil moisture and temperature were key determinants of GPP sensitivity to precipitation in Chinese agricultural systems. Additionally, changes in management practices and cropping patterns may contribute to increased GPP [52]. For forest areas, Li et al. identified precipitation, rather than temperature, as the climatic factor most affecting the interannual variation of forest GPP [53]. Additionally, afforestation projects promoted a shift from lower to higher forest GPP and supported a consistent increase in GPP, thereby enhancing its stability [54]. This study focuses on the effects of plant physiology and phenology on GPP changes but does not consider

the response of GPP to various ecological factors. Future studies should integrate these ecological factors into the model for comprehensive analysis.

Secondly, we used remotely sensed and modelled data as a source of data for the GPP in this study. Terrestrial ecosystem models have significant uncertainties in model structure, parameterization, and driving data, and the correction and deterministic assessment of model data become important scientific issues [55,56]. He et al. found significant overestimation or underestimation of GPP in both ISIMIP and MsTMIP models, particularly in low-GPP regions [11]. This discrepancy may stem from uncertainties in model input data as well as the model itself. Factors such as climate information, system noise, and processing bias can affect the accurate simulation of GPP at the regional scale [13,56]. Variations in climate input parameters can lead to differing GPP outputs for Chinese grasslands between the two model datasets. Additionally, differences in environmental drivers and related data—such as time-varying atmospheric CO_2 concentrations, nitrogen deposition, C3/C4 fractions, major crop distributions, phenology, and soil characteristics—also contribute to GPP over- or underestimation in model simulations [57]. We used remotely sensed and modelled data as a source of data for the GPP in this study; while ensemble average data reduced data uncertainty to some extent, the impact of internal model elements on GPP data was not addressed. Future uncertainty analyses should evaluate the influence of different model components to identify sources of uncertainty in GPP data.

5. Conclusions

This study analyzed the long-term trends of GPP and GPP_{max} across China's terrestrial ecosystems over the past 40 years by integrating results from two sets of terrestrial ecosystem models and two sets of remotely sensed datasets. Additionally, partial correlation analysis was used to examine the factors affecting inter-annual variations in GPP for these ecosystems; the study found different proportions of upward trends in GPP and GPP_{max} across various datasets. Among the multi-source data, the highest proportions of datasets with upward trends in China's grassland, cropland and forest were 81%, 98%, and 84%, respectively. The spatial patterns of GPP_{max} trends were closely related to those of overall GPP data. There was notable spatial heterogeneity in the trends of GPP and GPP_{max} derived from both models and remote sensing data. This finding underscored the insufficiency of relying on a single data source for a comprehensive analysis of GPP and GPP_{max} trends. To gain a detailed understanding of the spatial and temporal dynamics of ecosystem GPP in China, it is essential to compare multiple GPP datasets. Therefore, the study recommended using a combination of multiple data sources to evaluate the long-term dynamics of GPP. A comparison of the effect sizes of CUP and GPP_{max} on interannual GPP variations using partial correlation analyzes showed that GPP_{max} controlled interannual GPP variations in most areas of China's terrestrial ecosystems. This was particularly evident in grassland, where more than 99% of the inter-annual variation in grassland GPP was controlled by GPP_{max}. In conclusion, the integration of multiple data sources and the dominant role of GPP_{max} highlighted the complex and critical factors driving the inter-annual variations and long-term trends of GPP in China's terrestrial ecosystems.

Author Contributions: Conceptualization, L.L. and H.S.; methodology, H.S.; software, H.S. and Y.C. and Q.A.; writing and editing, H.S. and L.L. All authors contributed to the editing of the manuscript. All authors have read and agreed to the published version of the manuscript.

Data Availability Statement: No new data were created or analyzed in this study. Data sharing is not applicable to this article.

Surface Satellite (GLASS) team, and the Multisource Data Synergised Quantitative (MuSyQ) team, for making the data freely available.

Conflicts of Interest: The authors declare no conflicts of interest.

References

1. Wang, J.; Xie, Y.; Wang, X.; Dong, J.; Bie, Q. Detecting Patterns of Vegetation Gradual Changes (2001–2017) in Shiyang River Basin, Based on a Novel Framework. *Remote Sens.* **2019**, *11*, 2475. [CrossRef]
2. Chen, C.; Park, T.; Wang, X.; Piao, S.; Xu, B.; Chaturvedi, R.K.; Fuchs, R.; Brovkin, V.; Ciais, P.; Fensholt, R. China and India lead in greening of the world through land-use management. *Nat. Sustain.* **2019**, *2*, 122–129. [CrossRef] [PubMed]
3. Xia, J.; Niu, S.; Ciais, P.; Janssens, I.A.; Chen, J.; Ammann, C.; Arain, A.; Blanken, P.D.; Cescatti, A.; Bonal, D.; et al. Joint control of terrestrial gross primary productivity by plant phenology and physiology. *Proc. Natl. Acad. Sci. USA* **2015**, *112*, 2788–2793. [CrossRef] [PubMed]
4. Zhou, S.; Zhang, Y.; Ciais, P.; Xiao, X.M.; Luo, Y.Q. Dominant role of plant physiology in trend and variability of gross primary productivity in North America. *Sci. Rep. UK* **2017**, *7*, 41366. [CrossRef] [PubMed]
5. Jeong, S.J.; Ho, C.H.; Choi, S.D.; Kim, J.; Lee, E.J.; Gim, H.J. Satellite Data-Based Phenological Evaluation of the Nationwide Reforestation of South Korea. *PLoS ONE* **2013**, *8*, e58900. [CrossRef] [PubMed]
6. Suttie, J.M.; Reynolds, S.G.; Batello, C. *Grasslands of the World*; Food and Agriculture Organization: Rome, Italy, 2005.
7. Bulletin on the main data of the Third National Land Survey. *People's Daily*, (PRC newspaper 25/8/2021).
8. Wang, Q.; Zhang, Q.; Zhou, W. Grassland Coverage Changes and Analysis of the Driving Forces in Maqu County. *Phys. Procedia* **2012**, *33*, 1292–1297. [CrossRef]
9. He, P.; Ma, X.; Meng, X.; Han, Z.; Liu, H.; Sun, Z. Spatiotemporal evolutionary and mechanism analysis of grassland GPP in China. *Ecol. Indic.* **2022**, *143*, 109323. [CrossRef]
10. Xue, Y.; Liang, H.; Ma, Y.; Xue, G.; He, J. The Impacts of Climate and Human Activities on Grassland Productivity Variation in China. *Remote Sens.* **2023**, *15*, 3864. [CrossRef]
11. He, P.; Ma, X.; Han, Z.; Meng, X.; Sun, Z. Uncertainties of gross primary productivity of Chinese grasslands based on multi-source estimation. *Front. Environ. Sci.* **2022**, *10*, 928351. [CrossRef]
12. Huntzinger, D.N.; Schwalm, C.; Michalak, A.M.; Schaefer, K.; King, A.W.; Wei, Y.; Jacobson, A.; Liu, S.; Cook, R.B.; Post, W.M. The North American Carbon Program Multi-Scale Synthesis and Terrestrial Model Intercomparison Project—Part 1: Overview and experimental design. *Geosci. Model Dev.* **2013**, *6*, 2121–2133. [CrossRef]
13. Wei, L.; Huntzinger, D.N.; Michalak, A.M.; Viovy, P.; Schwalm, W.M. The North American Carbon Program Multi-scale Synthesis and Terrestrial Model Intercomparison Project—Part 2: Environmental driver data. *Geosci. Model. Dev.* **2014**, *7*, 2875–2893. [CrossRef]
14. Zhou, S.; Yu, B.; Schwalm, C.R.; Ciais, P.; Zhang, Y.; Fisher, J.B.; Michalak, A.M.; Wang, W.; Poulter, B.; Huntzinger, D.N.; et al. Response of Water Use Efficiency to Global Environmental Change Based on Output From Terrestrial Biosphere Models. *Glob. Biogeochem. Cycle.* **2017**, *31*, 1639–1655. [CrossRef]
15. Mao, J.; Thornton, P.E.; Shi, X.; Zhao, M.; Post, W.M. Remote Sensing Evaluation of CLM4 GPP for the Period 2000–2009*. *J. Clim.* **2012**, *25*, 5327–5342. [CrossRef]
16. Li, H.; Huang, M.; Wigmosta, M.S.; Ke, Y.; Coleman, A.M.; Leung, L.R.; Wang, A.; Ricciuto, D.M. Evaluating runoff simulations from the Community Land Model 4.0 using observations from flux towers and a mountainous watershed. *J. Geophys. Res. Atmos.* **2011**, *116*, D24120. [CrossRef]
17. Tian, H.; Chen, G.; Zhang, C.; Liu, M.; Sun, G.; Chappelka, A.; Ren, W.; Xu, X.; Lu, C.; Pan, S.; et al. Century-Scale Responses of Ecosystem Carbon Storage and Flux to Multiple Environmental Changes in the Southern United States. *Ecosystems* **2012**, *15*, 674–694. [CrossRef]
18. Jain, A.K.; Meiyappan, P.; Song, Y.; House, J.I. CO_2 emissions from land-use change affected more by nitrogen cycle, than by the choice of land-cover data. *Glob. Change Biol.* **2013**, *19*, 2893–2906. [CrossRef] [PubMed]
19. Rosenzweig, C.; Arnell, N.W.; Ebi, K.L.; Lotze-Campen, H.; Raes, F.; Rapley, C.; Smith, M.S.; Cramer, W.; Frieler, K.; Reyer, C.P.O.; et al. Assessing inter-sectoral climate change risks: The role of ISIMIP. *Environ. Res. Lett.* **2017**, *12*, 10301. [CrossRef]
20. Warnant, P.; Francois, L.; Strivay, D.; Gerard, J.C. CARAIB; a global model of terrestrial biological productivity. *Glob. Biogeochem. Cycle.* **1994**, *8*, 255–270. [CrossRef]
21. Smith, B.; Wårlind, D.; Arneth, A.; Hickler, T.; Leadley, P.; Siltberg, J.; Zaehle, S. Implications of incorporating N cycling and N limitations on primary production in an individual-based dynamic vegetation model. *Biogeosciences* **2014**, *11*, 2027–2054. [CrossRef]
22. Bondeau, A.; Smith, P.C.; Zaehle, S.; Schaphoff, S.; Lucht, W.; Cramer, W.; Gerten, D.; Lotze Campen, H.; Müller, C.; Reichstein, M.; et al. Modelling the role of agriculture for the 20th century global terrestrial carbon balance. *Glob. Change Biol.* **2007**, *13*, 679–706. [CrossRef]
23. Guimberteau, M.; Zhu, D.; Maignan, F.; Huang, Y.; Yue, C.; Dantec-Nédélec, S.; Ottlé, C.; Jornet-Puig, A.; Bastos, A.; Laurent, P.; et al. ORCHIDEE-MICT (v8.4.1), a land surface model for the high latitudes: Model description and validation. *Geosci. Model. Dev.* **2018**, *11*, 121–163. [CrossRef]

24. Zheng, Y.; Shen, R.; Wang, Y.; Li, X.; Liu, S.; Liang, S.; Chen, J.M.; Ju, W.; Zhang, L.; Yuan, W. Improved estimate of global gross primary production for reproducing its long-term variation, 1982–2017. *Earth Syst. Sci. Data.* **2020**, *12*, 2725–2746. [CrossRef]

25. Yuan, W.; Liu, S.; Zhou, G.; Zhou, G.; Tieszen, L.L.; Baldocchi, D.; Bernhofer, C.; Gholz, H.; Goldstein, A.H.; Goulden, M.L.; et al. Deriving a light use efficiency model from eddy covariance flux data for predicting daily gross primary production across biomes. *Agric. For. Meteorol.* **2007**, *143*, 189–207. [CrossRef]

26. Yuan, W.; Cai, W.; Xia, J.; Chen, J.; Liu, S.; Dong, W.; Merbold, L.; Law, B.; Arain, A.; Beringer, J.; et al. Global comparison of light use efficiency models for simulating terrestrial vegetation gross primary production based on the LaThuile database. *Agric. For. Meteorol.* **2014**, *192*, 108–120. [CrossRef]

27. Wang, M.; Sun, R.; Zhu, A.; Xiao, Z. Evaluation and Comparison of Light Use Efficiency and Gross Primary Productivity Using Three Different Approaches. *Remote Sens.* **2020**, *12*, 1003. [CrossRef]

28. Wang, J.; Sun, R.; Zhang, H.; Xiao, Z.; Zhu, A.; Wang, M.; Yu, T.; Xiang, K. New Global MuSyQ GPP/NPP Remote Sensing Products From 1981 to 2018. *IEEE J. Sel. Top. Appl. Earth Observ. Remote Sens.* **2021**, *14*, 5596–5612. [CrossRef]

29. Piao, S.; Fang, J.; Zhou, L.; Ciais, P.; Zhu, B. Variations in satellite-derived phenology in China's temperate vegetation. *Glob. Change Biol.* **2006**, *12*, 672–685. [CrossRef]

30. Cong, N.; Piao, S.; Chen, A.; Wang, X.; Lin, X.; Chen, S.; Han, S.; Zhou, G.; Zhang, X. Spring vegetation green-up date in China inferred from SPOT NDVI data: A multiple model analysis. *Agric. For. Meteorol.* **2012**, *165*, 104–113. [CrossRef]

31. Yin, Y.; Zhao, R.; Yang, Y.; Meng, Q.; Ying, H.; Cassman, K.G.; Cong, W.; Tian, X.; He, K.; Wang, Y.; et al. A steady-state N balance approach for sustainable smallholder farming. *Proc. Natl. Acad. Sci. USA* **2021**, *118*, 1. [CrossRef]

32. Bao, S.; Wutzler, T.; Koirala, S.; Cuntz, M.; Ibrom, A.; Besnard, S.; Walther, S.; Igut, L.; Moreno, A.; Weber, U. Environment-sensitivity functions for gross primary productivity in light use efficiency models. *Agric. For. Meteorol.* **2022**, *312*, 108708. [CrossRef]

33. Ma, J.; Xiao, X.; Miao, R.; Li, Y.; Chen, B.; Zhang, Y.; Zhao, B. Trends and controls of terrestrial gross primary productivity of China during 2000–2016. *Environ. Res. Lett.* **2019**, *14*, 84032. [CrossRef]

34. Weiwei, Q.I.; Haishan, N.; Shiping, W.; Yanjie, L.; Lirong, Z. Simulation of effects of warming on carbon budget in alpine meadow ecosystem on the Tibetan. *Acta Ecol. Sin.* **2012**, *32*, 1713–1722. [CrossRef]

35. Friedlingstein, P.O.M.J. Global Carbon Budget. *Sci. Data Earth Syst.* **2023**, *15*, 5301–5369. [CrossRef]

36. Han, J.; Guo, C.; Ye, S.; Zhang, L.; Li, S.; Wang, H.; Yu, G. Effects of diffuse photosynthetically active radiation on gross primary productivity in a subtropical coniferous plantation vary in different timescales. *Ecol. Indic.* **2020**, *115*, 106403. [CrossRef]

37. Liu, Y.; Zhou, R.; Ren, H.; Zhang, W.; Zhang, Z.; Zhang, Z.; Wen, Z. Evaluating the dynamics of grassland net primary productivity in response to climate change in China. *Glob. Ecol. Conserv.* **2021**, *28*, e01574. [CrossRef]

38. Gampe, D.; Zscheischler, J.; Reichstein, M.; O Sullivan, M.; Smith, W.K.; Sitch, S.; Buermann, W. Increasing impact of warm droughts on northern ecosystem productivity over recent decades. *Nat. Clim. Change* **2021**, *11*, 772–779. [CrossRef]

39. Fang, J.; Guo, Z.; Piao, S.; Chen, A. Terrestrial vegetation carbon sinks in China, 1981–2000. *Sci. China Ser. D Earth Sci.* **2007**, *50*, 1341–1350. [CrossRef]

40. Guirui, Y.; Xuanran, L.; Oiufeng, W.; Shenggong, L. Carbon Storage and Its Spatial Pattern of Terrestrial Ecosystem in China. *J. Resour. Ecol.* **2010**, *2*, 97–109.

41. Frankenberg, C.; Fisher, J.B.; Worden, J.; Badgley, G.; Saatchi, S.S.; Lee, J.; Toon, G.C.; Butz, A.; Jung, M.; Kuze, A.; et al. New global observations of the terrestrial carbon cycle from GOSAT: Patterns of plant fluorescence with gross primary productivity. *Geophys. Res. Lett.* **2011**, *38*, L17706. [CrossRef]

42. Piao, S.; He, Y.; Wang, X.; Chen, F. Estimation of China's terrestrial ecosystem carbon sink: Methods, progress and prospects. *Sci. China Earth Sci.* **2022**, *65*, 641–651. [CrossRef]

43. Zaehle, S.; Sitch, S.; Smith, B.; Hatterman, F. Effects of parameter uncertainties on the modeling of terrestrial biosphere dynamics. *Glob. Biogeochem. Cycle.* **2005**, *19*, GB3020. [CrossRef]

44. Huete, A.; Didan, K.; Miura, T.; Rodriguez, E.P.; Gao, X.; Ferreira, L.G. Overview of the radiometric and biophysical performance of the MODIS vegetation indices. *Remote Sens. Environ.* **2002**, *83*, 195–213. [CrossRef]

45. Piao, S.P.P.N. Growing season extension and its impact on terrestrial carbon cycle in the Northern Hemisphere over the past 2 decades. *Glob. Biogeochem. Cycle.* **2007**, *21*, GB3018. [CrossRef]

46. Starr, G.R.E.; Oberbauer, S.F.; Pop, E.R.I.C. Effects of lengthened growing season and soil warming on the phenology and physiology of Polygonum bistorta. *Glob. Change Biol.* **2010**, *6*, 357–369. [CrossRef]

47. Moors, E.J. Influence of spring and autumn phenological transitions on forest ecosystem productivity. *Philos. Trans. R. Soc. B Biol. Sci.* **2010**, *365*, 3227–3246.

48. Keenan, T.F.; Gray, J.; Friedl, M.A.; Toomey, M.; Bohrer, G.; Hollinger, D.Y.; Munger, J.W.; O Keefe, J.; Schmid, H.P.; Wing, I.S. Net carbon uptake has increased through warming-induced changes in temperate forest phenology. *Nat. Clim. Change* **2014**, *4*, 598–604. [CrossRef]

49. Zscheischler, J.; Reichstein, M.; Harmeling, S.; Rammig, A.; Tomelleri, E.; Mahecha, M.D. Extreme events in gross primary production: A characterization across continents. *Biogeosciences* **2014**, *11*, 2909–2924. [CrossRef]

50. Piao, S.; Wang, X.; Park, T. Characteristics, drivers and feedbacks of global greening. *Nat. Rev. Earth Environ.* **2020**, *1*, 14–27. [CrossRef]

51. Zhao, Y.; Peng, J.; Ding, Z.; Qiu, S.; Liu, X.; Wu, J.; Meersmans, J. Divergent dynamics between grassland greenness and gross primary productivity across China. *Ecol. Indic.* **2022**, *142*, 109100. [CrossRef]
52. Zhao, Y.; Wang, L.; Jiang, Q.; Wang, Z. Sensitivity of gross primary production to precipitation and the driving factors in China's agricultural ecosystems. *Sci. Total Environ.* **2024**, *948*, 174938. [CrossRef]
53. Li, Y.; Zhang, Y.; Lv, J. Interannual variations in GPP in forest ecosystems in Southwest China and regional differences in the climatic contributions. *Ecol. Inform.* **2022**, *69*, 101591. [CrossRef]
54. Liu, H.; Wang, Z.; Wang, Z.; Zeng, Y.; Xue, P.; Zhang, M. Stability of the ecosystem gross primary productivity increasing in Chinese forestry ecological engineering area. *Agric. Ecosyst. Environ.* **2023**, *356*, 108636. [CrossRef]
55. Shao, J.; Zhou, X.; Luo, Y.; Zhang, G.; Yan, W.; Li, J.; Li, B.; Dan, L.; Fisher, J.B.; Gao, Z. Uncertainty analysis of terrestrial net primary productivity and net biome productivity in China during 1901–2005. *J. Geophys. Res. Biogeosci.* **2016**, *121*, 1372–1393. [CrossRef]
56. Cheng, S.; Huang, J.; Ji, F.; Lin, L. Uncertainties of soil moisture in historical simulations and future projections. *J. Geophys. Res.-At.* **2017**, *122*, 2239–2253. [CrossRef]
57. Exbrayat, J.; Bloom, A.A.; Falloon, P.; Ito, A.; Smallman, T.L.; Williams, M. Reliability ensemble averaging of 21st century projections of terrestrial net primary productivity reduces global and regional uncertainties. *Earth Syst. Dyn.* **2018**, *9*, 153–165. [CrossRef]